

Comparison of *Gaia* DR2 Parallaxes of Stars with VLBI Astrometry

SHUANGJING XU (徐双敬),^{1,2} BO ZHANG (张波),¹ MARK J. REID,³ XINGWU ZHENG (郑兴武),⁴ AND
GUANGLI WANG (王广利)^{1,2}

¹*Shanghai Astronomical Observatory, Chinese Academy of Sciences, 80 Nandan Road, Shanghai 200030, China*

²*University of Chinese Academy of Sciences, 19A Yuquanlu, Beijing 100049, China*

³*Center for Astrophysics | Harvard & Smithsonian, 60 Garden Street, Cambridge, MA 02138, USA*

⁴*School of Astronomy and Space Science, Nanjing University, 22 Hankou Road, Nanjing 210093, China*

ABSTRACT

We compare the parallaxes of stars from VLBI astrometry in the literature to those in the *Gaia* DR2 catalog. Our full sample contains young stellar objects, evolved AGB stars, pulsars and other radio stars. Excluding AGB stars, which show significant discrepancies between *Gaia* and VLBI parallaxes, and stars in binary systems, we obtain an average, systematic, parallax offset of $-75 \pm 29 \mu\text{as}$ for *Gaia* DR2, consistent with their estimate of a parallax zero-point between -100 and $0 \mu\text{as}$.

1. INTRODUCTION

The second data release (DR2) of *Gaia* provides precise celestial coordinates, trigonometric parallaxes, and proper motions for more than 1.3 billion stars based on observations collected during the first 22 months of the mission (since July 2014) (Gaia Collaboration et al. 2018). However, there are systematic astrometric errors in *Gaia* DR2. The astrometric uncertainties of celestial objects provided in *Gaia* DR2 are mainly depended on their magnitudes and celestial positions owing to the scanning law of *Gaia* (Lindgren et al. 2018). For parallaxes, uncertainties are typical ~ 0.04 , 0.1 and 0.7 mas for stars with G magnitude $\leq \sim 14$, 17 and 20 , respectively (Luri et al. 2018). Similarly to *Gaia* DR1, all sources are treated as single stars and thus representable by five astrometric parameters associated with parallax and proper motion. For unresolved binaries (separation ≤ 100 mas), the results thus refer to the photo-center, and orbital motion and photometric variability may corrupt the astrometric parameters. For resolved binaries, the results may refer to either component and are sometimes spurious due to confusion of the components. Based on quasars and validation solutions, Lindgren et al. (2018) estimate that the zero-point parallax corrections depend on position, magnitude, and color and are generally below $100 \mu\text{as}$ in magnitude, with an average bias of about $-29 \mu\text{as}$.

Clearly, independent assessments of *Gaia* parallaxes are important to fully characterize systematic errors. Stassun & Torres (2018) find a parallax zero-point of $-82 \pm 33 \mu\text{as}$ based on 89 eclipsing binaries. Zinn et al. (2018) present an independent confirmation of parallax zero-point of $-52.8 \pm 2.4 \mu\text{as}$ (stat.) $\pm 1 \mu\text{as}$ (syst.) based on 3500 evolved stars in the *Kepler* field. Riess et al. (2018) find the parallax offset to be $-46 \pm 13 \mu\text{as}$ based on the *Hubble Space Telescope* (*HST*) data of 50 long-period Galactic Cepheids. Based on a direct comparison of the *Gaia* DR2 with VLBA parallaxes for 55 young stars, Kounkel et al. (2018) find a parallax zero-point of $-73 \pm 34 \mu\text{as}$. Bobylev (2018) also estimates a parallax zero-point of $-38 \pm 46 \mu\text{as}$ using a sample of 75 radio stars with *Gaia* DR2 and VLBI measurements. All of these estimated zero-points are larger than the *Gaia* average value of $-29 \mu\text{as}$. However, the stars from the above-mentioned comparisons are either a specific stellar class of stars or from a specific region within a limited distant range and some of the astrometric results are not from trigonometric parallax measurement. Therefore, a comparison using stars of different types with independent trigonometric parallaxes could robustly assess the *Gaia* DR2 parallax zero-point issue.

Very Long Baseline Interferometry (VLBI) astrometry is capable of measuring parallaxes with accuracies of $\sim 10 \mu\text{as}$ (Reid & Honma 2014), which is comparable to or better than the goals of *Gaia*. Because radio waves are not absorbed significantly by interstellar dust, the entire Milky Way is available for VLBI observation. Such measurements have now been carried out for hundreds of radio sources as distant as 20 kpc (Sanna et al. 2017). Since VLBI astrometry

is relative to distant quasars, the results are absolute parallaxes with no significant zero-point correction. Thus, in order to perform an independent assessment of *Gaia* DR2 parallaxes directly, we collected a sample of ~ 100 stars of different types with published VLBI parallaxes. Most of the VLBI parallax uncertainties in the sample are smaller than those of the *Gaia* DR2, which offers a unique opportunity to assess *Gaia* DR2 parallaxes, particularly for the *Gaia* parallaxes zero-point.

2. DATA

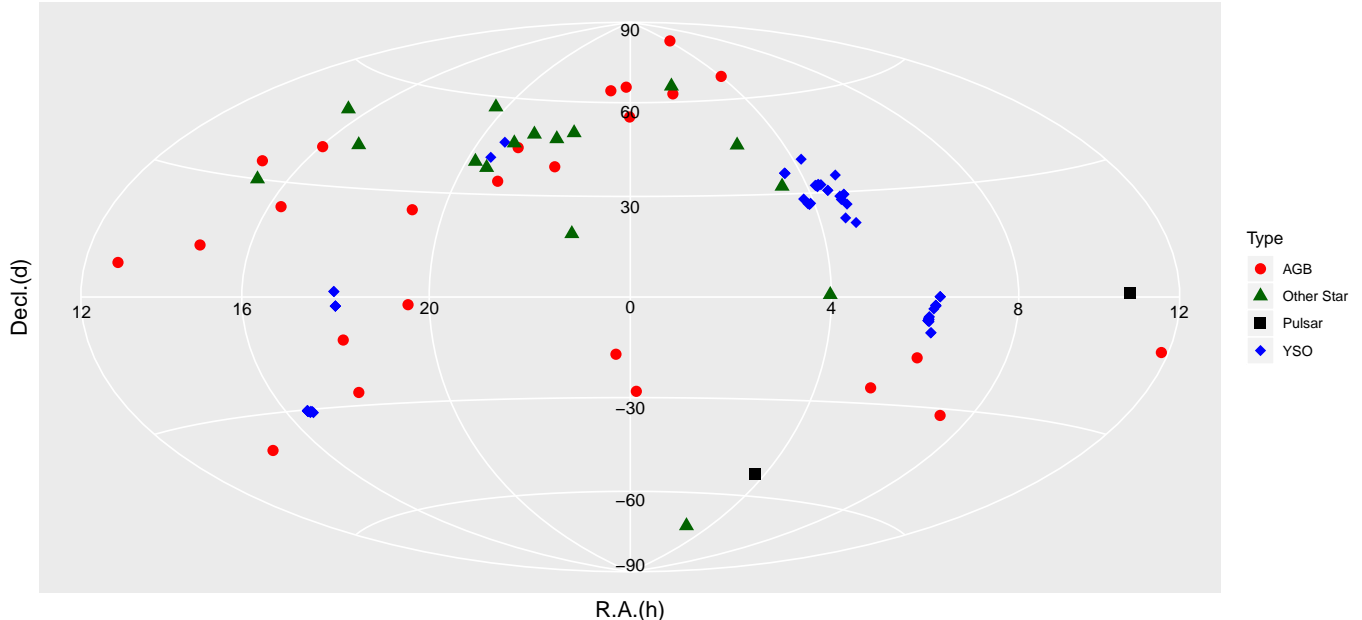


Figure 1. The sky distribution of the stars with both VLBI and *Gaia* DR2 parallaxes.

In Table 1, we compile a catalog of 108 stars with both VLBI and *Gaia* DR2 astrometric results. The sky distribution of these stars are shown in Figure 1, with most of the stars in or near the Galactic plane. We assembled this catalog by starting with more than 130 stars with VLBI parallax results and finding that 93 already have *Gaia* DR2 results be identified in the SIMBAD database (Wenger et al. 2000). The methods used for the cross-identification of SIMBAD with *Gaia* DR2 by Simbad Team are as follows: (1) Objects must have pre-*Gaia* sub-arcsecond accurate coordinates in SIMBAD; (2) Coordinates of *Gaia* objects were calculated at epoch 2000.0 taking into account their measured proper motions in order to be compared to the positions in SIMBAD; (3) *Gaia* stars were discarded if they have a neighbouring star in SIMBAD closer than $3''$; (4) SIMBAD stars were also discarded if they have a neighbouring star at less than $3''$ in *Gaia* DR2, with a difference of magnitude of < 3 mag, the brighter source being at less than $1''$ from the SIMBAD position; (5) Finally SIMBAD stars that were cross-identified with a *Gaia* DR2 source with a positional difference $> 1.0''$ were also discarded. Additionally, we found 15 VLBI/*Gaia* stars that do not appear in SIMBAD. Among them there are seven stars (IRAS 18286-0959, bet Per, GBS-VLA J183123.62-020535.8, 2MASS J16264923-2420029, V1098 Tau, XZ Tau, & V1000 Tau) with null values for *Gaia* parallaxes and one star (VY CMA) with a negative *Gaia* parallax, and we do not use them in the comparison.

For VLBI parallaxes, there are 15 stars with more than one parallax measurement, and for these used variance-weighted averaged results. The stellar parallaxes listed in Table 1 range from ≈ 0.26 to 93.14 mas, corresponding to distances from ≈ 4 to 0.011 kpc. The median uncertainties of these VLBI and *Gaia* DR2 parallaxes are 74 and 123 μas , respectively. The stars in our sample include a number of stellar types, including YSOs, AGB stars, pulsars and other radio stars.

3. COMPARISON OF VLBI AND *Gaia* DR2 PARALLAXES

The astrometric results for pulsars in *Gaia* DR2 are from binary companions (Jennings et al. 2018). We find that the parallax result of PSR J1023+0038 is consistent between VLBI and *Gaia* DR2, but there is a very large discrepancy for PSR J0437-4715. Since this sub-sample is small and unreliable, owing to the unmodeled effects of binary orbits on parallax, we do not consider them further in our analysis.

We examined three independent sub-samples of stars of different stellar types in order to compare the astrometric results of VLBI and *Gaia* DR2. Our sub-samples are as follows:

1. AGB: all AGB stars.
2. YSO: all YSO stars.
3. “Other”: the remaining stars in the Table 1.

In addition, we consider three groupings of these sub-samples:

4. AGB+YSO: the union of the AGB and YSO sub-samples.
5. YSO+”Other”: the union of the YSO and Other sub-samples.
6. Full: the union of the AGB, YSO and Other sub-samples.

Since we expect some outliers in the *Gaia* DR2 catalog (eg, from binaries), we use “box” plots (Tukey 1977; Feigelson & Babu 2012), a compact display of robust measures of location and spread, to identify and remove outliers. Figure 2 plots parallax and proper motion differences between the DR2 and VLBI measurements for our full sample. The boxes denote the inner quartile range (*IQR*), and the vertical red dashed-lines at $\pm 3.0 \times IQR$, separate the extreme outliers from the rest of the data. There are 5, 7 and 6 extreme outliers in the discrepancies of ϖ , μ_x and μ_y , respectively. These were separately removed from the statistics of each parameter, so that, for example, a proper motion parameter was still used for a star with a parallax outlier that was removed from the parallax statistics.

In order to fit the relationship between the VLBI and *Gaia* DR2 results, we adopt linear regression for data with errors in both X and Y axes, following the method derived by Deming (1943) and described in detail in York et al. (2004). We estimate the slope, intercept, and standard errors of the best straight line by minimizing the sum:

$$\chi^2 = \sum_{k=1}^n \left[\frac{(X_k - x_k)^2}{\sigma_{X,k}^2} + \frac{(Y_k - y_k)^2}{\sigma_{Y,k}^2} \right] \quad (1)$$

where (X_k, Y_k) denote the k^{th} data pair with corresponding standard deviations $(\sigma_{X,k}, \sigma_{Y,k})$ and (x_k, y_k) denote points of the estimated straight line. The best linear fit results are listed in Table 2 & 3. Figure 3 & 4 show the direct comparison of the VLBI and *Gaia* DR2 results.

As shown in Table 2, the agreement between the *Gaia* DR2 and VLBI parallaxes is excellent for all sub-samples, with the slopes of the fitted lines consistent with unity within 2σ uncertainties. The (y-axis) intercepts are small and negative, indicating the *Gaia* parallaxes are systematically smaller than the (absolute) VLBI parallaxes, as expected for the *Gaia* DR2 catalog.

Among all the samples, the AGB sample has the largest uncertainties and discrepancies between *Gaia* DR2 and VLBI data. Stellar angular diameters for 12 AGB stars from literature are listed in Table 4. In Figure 5, we plot the *Gaia* DR2 and VLBI parallax uncertainties for these AGB stars versus their angular diameters. There is a clear trend that the larger of the stellar size, the larger of the stellar parallax uncertainty for *Gaia* DR2, while there is no such a trend for VLBI observations. This is not unexpected for stars with angular sizes comparable to their parallaxes and known to have significant surface brightness variations.

As mentioned by Luri et al. (2018), the systematic errors in *Gaia* DR2 are complicated, affected by position on the sky, magnitude, and color. Mowlavi et al. (2018) claimed that the precision reached on the parallax depends on the $G_{BP}-G_{RP}$ color for long period variable candidates, where the G_{BP} and G_{RP} are the *Gaia* magnitudes of blue and red photometer values, respectively. The $G_{BP}-G_{RP}$ spread originates from extinction due to interstellar and/or circumstellar dust (Mowlavi et al. 2018). As shown in Figure 6, the parallax uncertainties of *Gaia* DR2 are larger than VLBI at magnitude > 16 and large $G_{BP}-G_{RP}$. This shows that redder AGB stars give larger parallax uncertainties; possible reasons include 1) they tend to be larger, 2) they probably have more surface brightness variations, and 3)

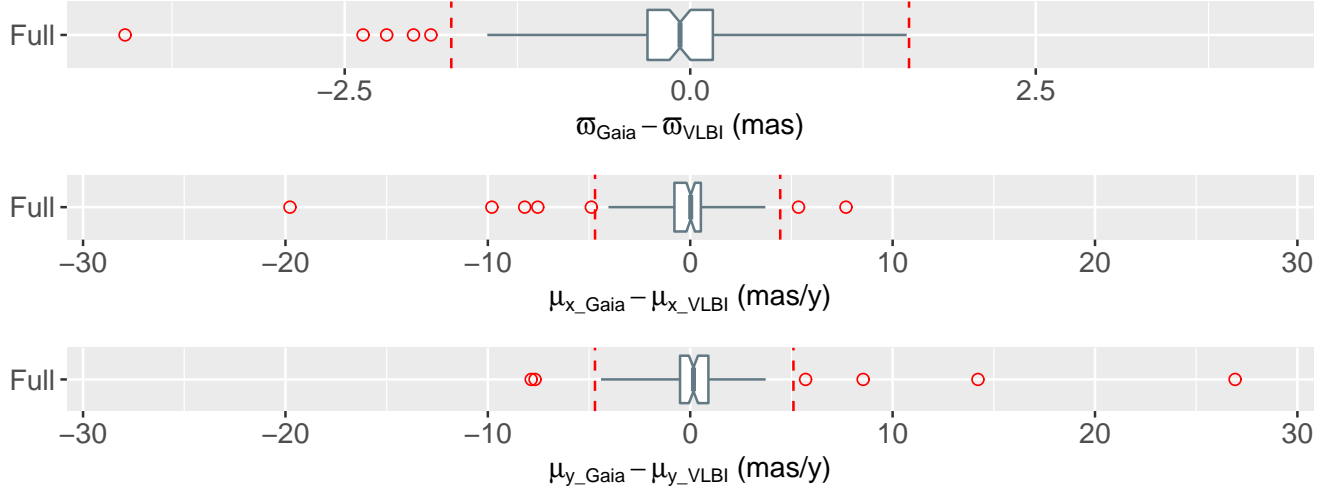


Figure 2. Box plots of differences between *Gaia* DR2 and VLBI for parallax, ϖ , (*upper panel*), eastward motion, μ_x , (*middle panel*) and northward motion, μ_y , (*lower panel*). The vertical boundaries (“hinges”) indicate the interquartile range (IQR). The notches on the sides of the box hinges are at $\pm 1.58 \times IQR/\sqrt{N}$, representing the standard deviation of the median for a Gaussian distribution. Vertical dashed red lines are set at $3.0 \times IQR$ above and below the 25% and 75% quartiles based on the Full sample. Extreme outliers fall outside the vertical dashed red lines and were excluded from our analysis.

Table 2. *Gaia* DR2 versus VLBI parallaxes

Sample	Including Binary?	Number ^a	ϖ		ϖ
			Slope	Intercept (mas)	Weighted mean ^b (mas)
AGB	YES	19	1.008 ± 0.080	-0.001 ± 0.105	$+0.006 \pm 0.078$
	NO	18	1.069 ± 0.078	-0.036 ± 0.094	$+0.023 \pm 0.070$
YSO	YES	59	0.999 ± 0.010	-0.057 ± 0.055	-0.062 ± 0.026
	NO	33	0.985 ± 0.012	-0.009 ± 0.059	-0.076 ± 0.029
Other	YES	15	1.004 ± 0.003	-0.103 ± 0.050	-0.075 ± 0.047
	NO	1			
AGB+YSO	YES	78	0.996 ± 0.009	-0.037 ± 0.046	-0.055 ± 0.024
	NO	51	0.984 ± 0.010	$+0.003 \pm 0.047$	-0.061 ± 0.027
YSO+Other	YES	74	1.003 ± 0.003	-0.080 ± 0.028	-0.065 ± 0.022
	NO	34	0.986 ± 0.011	-0.011 ± 0.058	-0.075 ± 0.029
Full	YES	93	1.002 ± 0.003	-0.069 ± 0.027	-0.059 ± 0.022
	NO	52	0.984 ± 0.010	$+0.001 \pm 0.047$	-0.061 ± 0.027

^aThe number of stars with outliers removed in each sample.

^bVariance weighting as $1/(\sigma_{\varpi_{VLBI}}^2 + \sigma_{\varpi_{Gaia}}^2)$

they will likely have more circumstellar dust to corrupt their images. We conclude that one should be cautious when using the *Gaia* parallaxes for AGB stars.

Certainly, binaries can yield unreliable parallaxes, since unmodeled orbital motions can be significant. Note that the sub-samples excluding binaries have larger slope uncertainties than samples including binaries. This is simply a result of much larger parallax range of ~ 93 mas for samples including binaries than ~ 8 mas when the binaries are excluded as shown in Figure 3.

For our most reliable estimate of the *Gaia* DR2 parallax zero-point we choose the results of the YSO+Other samples that exclude binaries and red giants. Assuming that the slopes are exactly unity, we can simply calculate a variance-weighted mean difference between DR2 and VLBI parallaxes in order to estimate the *Gaia* zero-point correction. These are also shown in Table 2. We find the zero-point is $-75 \pm 29 \mu\text{as}$ if the slope is assumed to be exactly unity. The

Table 3. Proper motions of *Gaia* DR2 versus VLBI

Sample	Including Binary?	Number ^a	μ_x^c			μ_y^c			
			Slope	Intercept (mas yr ⁻¹)	Weighted mean ^b (mas yr ⁻¹)	Slope	Intercept (mas yr ⁻¹)	Weighted mean ^b (mas yr ⁻¹)	
AGB	YES	20	1.000 ± 0.025	+0.346 ± 0.254	+0.354 ± 0.249	23	0.995 ± 0.032	+0.430 ± 0.396	+0.464 ± 0.318
	NO	20	1.000 ± 0.025	+0.346 ± 0.254	+0.354 ± 0.249	22	0.985 ± 0.034	+0.398 ± 0.397	+0.503 ± 0.325
YSO	YES	57	0.988 ± 0.006	-0.029 ± 0.098	-0.038 ± 0.102	55	1.008 ± 0.011	-0.014 ± 0.213	-0.130 ± 0.141
	NO	33	0.985 ± 0.011	+0.071 ± 0.124	-0.001 ± 0.114	31	0.996 ± 0.007	-0.046 ± 0.137	+0.011 ± 0.100
Other	YES	14	1.004 ± 0.001	-0.169 ± 0.085	-0.282 ± 0.129	14	1.000 ± 0.003	+0.103 ± 0.129	+0.105 ± 0.126
	NO	1				1			
AGB+YSO	YES	77	0.988 ± 0.006	-0.002 ± 0.088	-0.010 ± 0.091	78	1.009 ± 0.010	+0.038 ± 0.182	-0.089 ± 0.123
	NO	53	0.985 ± 0.010	+0.103 ± 0.104	+0.042 ± 0.100	53	0.998 ± 0.007	+0.047 ± 0.142	+0.078 ± 0.105
YSO+Other	YES	71	1.003 ± 0.001	-0.091 ± 0.079	-0.126 ± 0.081	69	1.002 ± 0.005	-0.049 ± 0.133	-0.081 ± 0.115
	NO	34	0.985 ± 0.011	+0.071 ± 0.122	-0.003 ± 0.112	32	0.996 ± 0.006	-0.039 ± 0.134	+0.014 ± 0.098
Full	YES	91	1.003 ± 0.001	-0.069 ± 0.072	-0.103 ± 0.075	92	1.003 ± 0.005	-0.016 ± 0.120	-0.051 ± 0.104
	NO	54	0.985 ± 0.009	+0.103 ± 0.103	+0.040 ± 0.099	54	0.998 ± 0.007	+0.051 ± 0.141	+0.081 ± 0.104

^a The number of stars with outliers removed in each sample.

^b Variance weighting as $1/(\sigma_{\mu_x \text{VLBI}}^2 + \sigma_{\mu_x \text{Gaia}}^2)$ and $1/(\sigma_{\mu_y \text{VLBI}}^2 + \sigma_{\mu_y \text{Gaia}}^2)$

^c $\mu_x = \mu_\alpha \cos \delta$, $\mu_y = \mu_\delta$

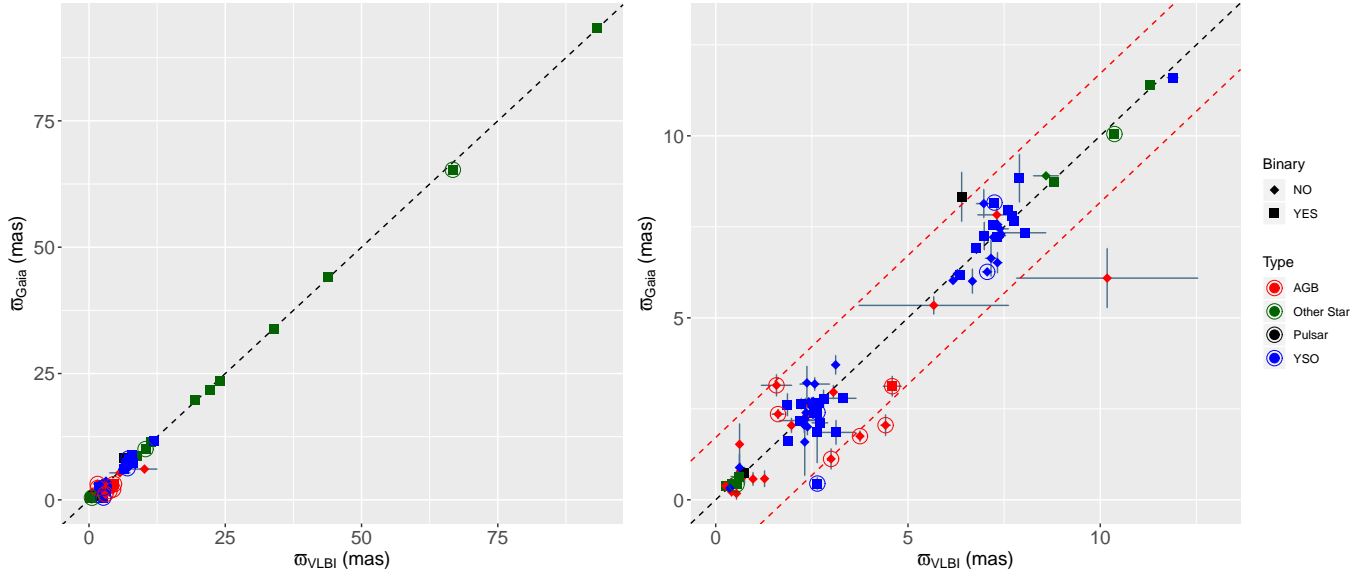


Figure 3. *Gaia* DR2 versus VLBI parallaxes. *Left panel:* all stars in the sample; *right panel:* stars with $\varpi < 13$ mas. Colors denote different stellar types and known binaries are shown in different shapes, as indicated in the legend at the right. Circles denote differences of $> 3\sigma$, where $\sigma = \sqrt{\sigma_{\varpi \text{VLBI}}^2 + \sigma_{\varpi \text{Gaia}}^2}$. The black dashed line is a fit with slope of 1 and intercept of 0. The red dashed lines in right panel separate extreme outliers as shown in Figure 2.

magnitude of our estimated parallax zero-point is statistically consistent, but perhaps larger than that of the *Gaia* DR2 claim of an overall parallax zero-point of $-29 \mu\text{as}$.

As shown in Table 3 and Figure 4, the fractional uncertainties of proper motions differences, while excellent, is not as good as for the parallaxes. Our results are independent of those estimated by [Stassun & Torres \(2018\)](#), [Zinn et al. \(2018\)](#) and [Riess et al. \(2018\)](#) as mentioned in § 1, since the stars and the methods for deriving parallaxes are different. In contrast to the results of the [Bobylev \(2018\)](#) and [Kounkel et al. \(2018\)](#), we use a larger sample of stars with VLBI parallaxes and consider the problems of AGB stars and binaries. There are 81 overlapping stars in Bobylev’s sample (88 stars) and our sample (108 stars); the remaining 7 stars in Bobylev’s sample had no VLBI parallax results, but were in

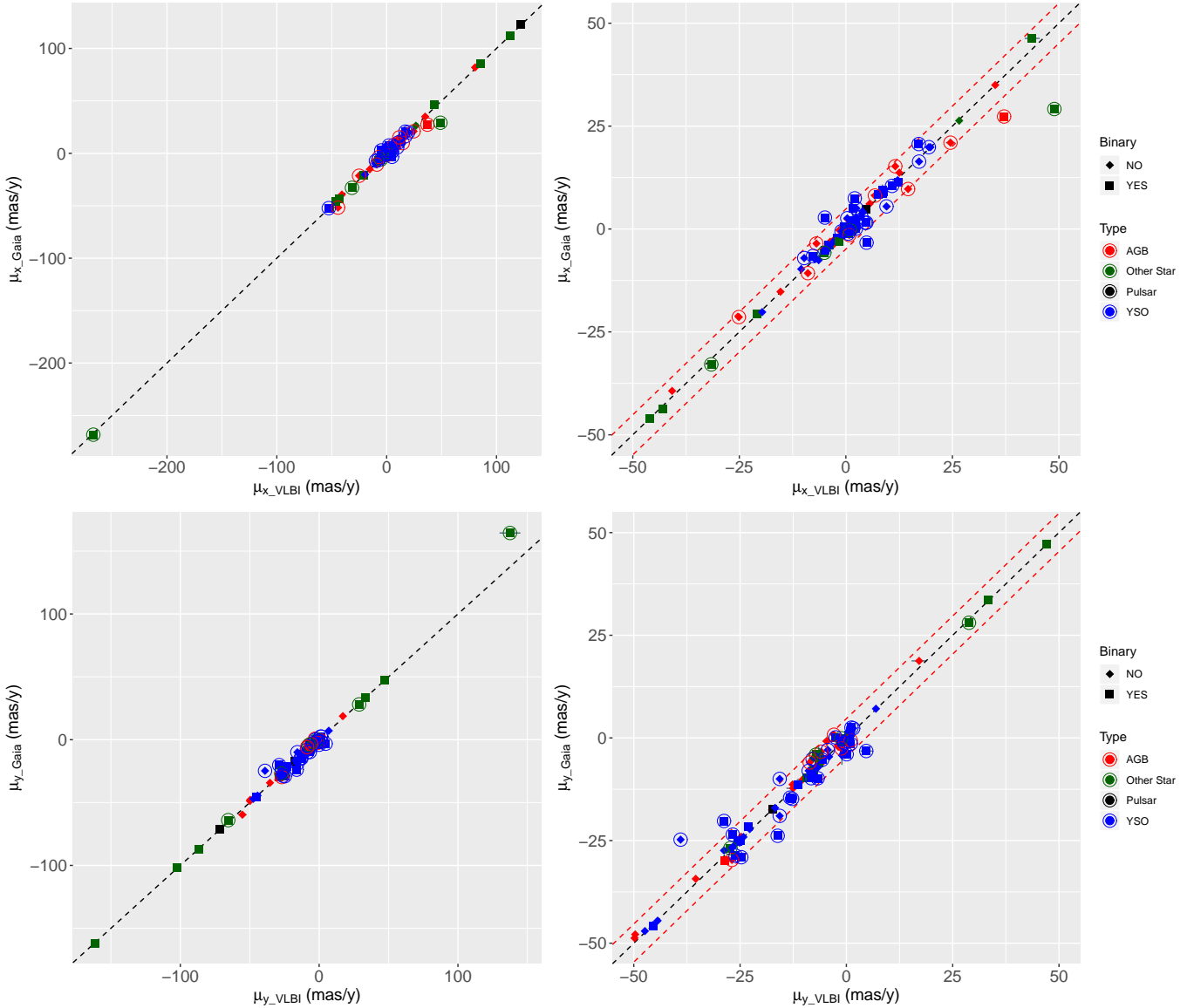


Figure 4. *Gaia* DR2 versus VLBI proper motions. *Left panels:* all stars in the sample; *right panels:* stars with proper motion components < 50 mas/yr in magnitude in the eastward *top* and northward *bottom* directions. Colors denote different stellar types and binaries are shown in different shapes, as indicated in the legend at the right. Circles denote differences of $> 3\sigma$, where for each coordinate $\sigma = \sqrt{\sigma_{\mu_{\text{VLBI}}}^2 + \sigma_{\mu_{\text{Gaia}}}^2}$. The black dashed line is a straight line with slope of 1 and intercept of 0. The red dashed lines in right panel separate extreme outliers as shown in Figure 2.

the sample as they had proper motions. Also, Bobylev did not perform a rigorous least-squares analysis that takes into account errors in both axes. Finally, [Bobylev \(2018\)](#) calculated the weighted mean with weights inversely proportional to the measurement errors $1/\sqrt{\sigma_{\varpi_{\text{VLBI}}}^2 + \sigma_{\varpi_{\text{Gaia}}}^2}$, whereas we use the variance weighting $1/(\sigma_{\varpi_{\text{VLBI}}}^2 + \sigma_{\varpi_{\text{Gaia}}}^2)$. Using our methods on Bobylev’s sample, we estimate the parallax zero-point as $-65 \pm 34 \mu\text{as}$ with 28 stars (i.e., excluding AGB and binary stars), which is consistent with our result.

4. SUMMARY

Based on the comparison of stellar parallaxes from *Gaia* DR2 and the generally more accurate VLBI values, we find a *Gaia* parallax zero-point correction of $-75 \pm 29 \mu\text{as}$. This value is consistent with published *Gaia* estimates that the zero-point is negative and below $100 \mu\text{as}$ in magnitude. We find that AGB stars have the largest discrepancies in both parallax and proper motions of the samples we consider. This is reasonable since AGB stars are generally large,

Table 4. Angular diameters AGB stars

Num	SIMBAD Name	Angular Diameter (mas)	Reference
1	S Crt	5.6 ± 1	Nakagawa et al. (2008)
2	S Per	6.6 ± 2.5	Richards et al. (2012)
3	SY Scl	3.8	Nyu et al. (2011)
4	NML Cyg	22	Zhang et al. (2012b)
5	VY CMa	20	Monnier et al. (2000)
6	PZ Cas	5.2 ± 1.2	Levesque et al. (2005)
7	R Aqr	17.7	Millan-Gabet et al. (2005)
8	T Lep	5.5 ± 2.4	Le Bouquin et al. (2009)
9	RW Lep	6.4	Kamezaki et al. (2014)
10	U Lyn	4.6 ± 0.4	Kamezaki et al. (2016b)
11	RT Vir	7.1 ± 0.4	Richards et al. (2012)
12	VX Sgr	9.5 ± 0.9	Richards et al. (2012)

NOTE—Some angular diameters are derived from stellar radii and VLBI distances.

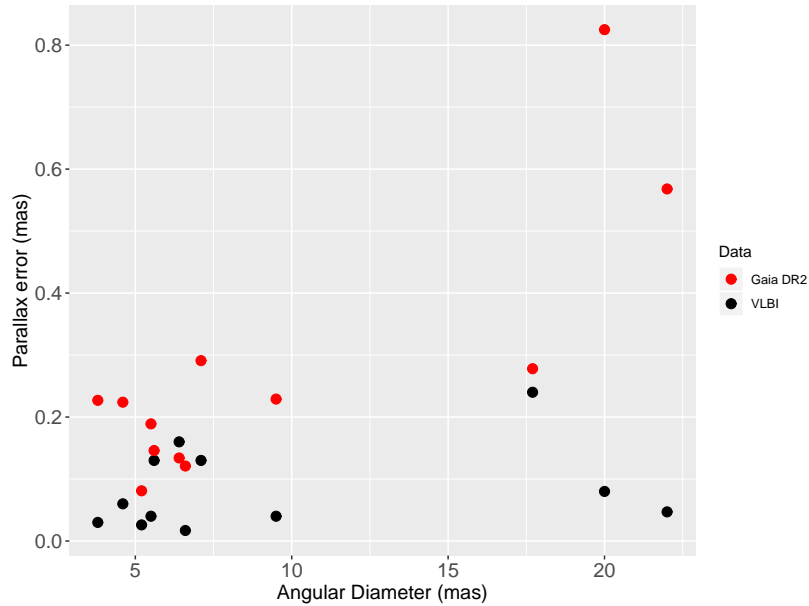


Figure 5. Parallax uncertainties versus angular diameters for AGB stars. *Red* and *black dots* denote *Gaia* DR2 and VLBI parallaxes, respectively.

variable, and often surrounded by copious dust. Radio observations of circumstellar masers for AGB stars can yield parallax accuracy roughly an order-of-magnitude better than *Gaia* DR2 (Zhang et al. 2017; Xu et al. 2018). In the future, with improvement in sensitivity and calibration of VLBI arrays, it should be feasible to detect weaker radio stars and provide a better assessment of *Gaia* parallax accuracy.

This work was partly supported by the 100 Talents Project of the Chinese Academy of Sciences, the National Science Foundation of China under grant 11673051, 11873077 and U1831136, and the Key Laboratory for Radio Astronomy, Chinese Academy of Sciences.

Facilities: *Gaia*, VLBA, VERA, EVN, LBA

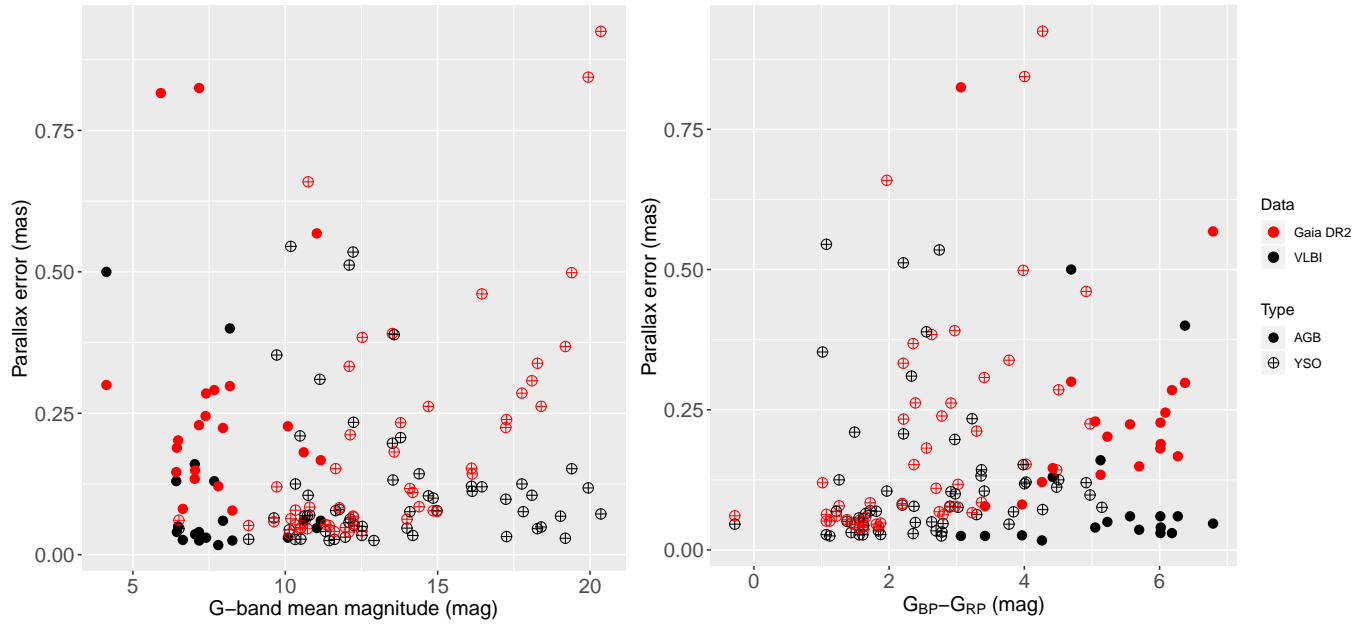


Figure 6. *Left panel* Parallax uncertainty versus G-band mean magnitude. *Right panel* Parallax uncertainty versus color ($G_{BP}-G_{RP}$). G_{BP} and G_{RP} are the *Gaia* magnitudes of the blue and red photometer, respectively.

Software: R (R Core Team 2013), TOPCAT (Taylor 2005).

Table 1. Parallaxes of *Gaia* DR2 and VLBI

Num	Main name in SIMBAD	Binary	Type	VLBI ϖ	VLBI μ_x	VLBI μ_y	Ref. ^a	<i>Gaia</i> ϖ	<i>Gaia</i> μ_x ^b	<i>Gaia</i> μ_y ^b	Noise _{sig} ^c	Gmag ^d	bp _{rp} ^e
				(mas)	(mas yr ⁻¹)	(mas yr ⁻¹)		(mas)	(mas yr ⁻¹)	(mas yr ⁻¹)		(mag)	(mag)
1	R Cas		AGB	5.67±1.95	80.52±2.35	17.1±1.75	5	5.342±0.245	81.92±0.403	18.76±0.358	1.77	7.383	6.086
2	W Hya		AGB	10.18±2.36	-44.24±2.04	-55.28±2.93	5	6.091±0.816	-51.773±1.298	-59.688±1.256	3.327	5.915	
3	S CrB		AGB	2.31±0.33	-9.08±0.27	-12.49±0.33	5	2.322±0.285	-10.731±0.473	-11.348±0.366	0.882	7.4	6.183
3				2.39±0.17	-8.58±0.38	-13.21±0.61	8						
4	U Her		AGB	3.61±1.04	-14.94±0.38	-9.17±0.42	5	1.749±0.149	-15.241±0.213	-10.141±0.227	0.696	7.04	5.698
4				3.76±0.27	-16.99±0.77	-11.88±0.5	8						
5	RR Aql		AGB	1.58±0.4	-25.11±0.74	-49.82±0.54	8	3.146±0.298	-21.397±0.481	-48.743±0.293	1.001	8.182	6.376
6	S Crt		AGB	2.33±0.13	-3.17±0.22	-5.41±0.22	12	2.646±0.146	-4.039±0.242	-4.95±0.153	0.539	6.421	4.42
7	R Aqr	Binary ^f	AGB	4.59±0.24	37.13±0.47	-28.62±0.44	32	3.122±0.278	27.33±0.423	-29.859±0.397	0.947	7.032	5.803
8	SY Scl		AGB	0.75±0.03	5.57±0.04	-7.32±0.12	21	0.675±0.227	6.111±0.326	-7.475±0.29	0.728	10.085	6.013
9	RX Boo		AGB	7.31±0.5	24.55±1.06	-49.67±2.38	26	7.829±0.3	20.978±0.515	-47.861±0.5	1.651	4.129	4.692
10	T Lep		AGB	3.06±0.04	14.6±0.5	-35.43±0.79	33	2.959±0.189	9.713±0.24	-34.322±0.238	0.771	6.442	6.017
11	RW Lep		AGB	1.62±0.16	12.55±0.59	-26.92±0.68	34	2.355±0.134	13.689±0.231	-29.712±0.25	0.548	7.029	5.127
12	U Lyn		AGB	1.27±0.06	0.8±0.57	-6±0.56	37	0.58±0.224	-1.457±0.208	-6.297±0.22	0.38	7.955	5.563
13	R UMa		AGB	1.97±0.05	-40.77±0.39	-24.75±0.38	39	2.045±0.202	-39.334±0.389	-24.059±0.351	0.559	6.484	5.228
14	RT Vir		AGB	4.417±0.13	35.056±0.697	-17.5±0.7	43	2.05±0.291	34.982±0.624	-17.552±0.612	1.509	7.668	
15	VX Sgr		AGB	0.64±0.04	0.36±0.76	-2.92±0.78	45	0.787±0.229	2.451±0.45	0.771±0.397	0.907	7.167	5.048
16	VY CMa		AGB	0.83±0.08	-2.8±0.2	2.6±0.2	23	-5.917±0.825	0.926±1.772	-6.474±1.754	4.484	7.173	3.061
16				0.88±0.08	-1.882±0.144	1.02±0.61	11						
17	NML Cyg		AGB	0.62±0.047	-1.55±0.42	-4.59±0.41	22	1.526±0.568	-0.268±1.124	-0.863±1.179	3.952	11.033	6.791
18	S Per		AGB	0.413±0.017	-0.49±0.23	-1.19±0.2	17	0.222±0.121	-0.01±0.295	-2.57±0.307	0.446	7.8	4.26
19	UX Cyg		AGB	0.54±0.06	-6.91±0.75	-12.52±1.57	7	0.176±0.167	-3.529±0.307	-12.266±0.402	0.586	11.164	6.27
20	FV Boo		AGB	0.97±0.06	6.81±0.14	1.01±0.12	38	0.573±0.181	8.121±0.319	-0.602±0.298	0.644	10.605	6.011
21	PZ Cas		AGB	0.356±0.026	-3.7±0.2	-2±0.3	28	0.42±0.081	-3.11±0.118	-1.808±0.11	0.381	6.637	3.965
22	IRAS 18286-0959		AGB	0.277±0.041	-3.152±0.295	-7.2±0.2	30				0.0	19.97	2.035
23	IRC +60370		AGB	0.4±0.025	-1.278±0.164	-1.91±0.17	27	0.479±0.078	-2.655±0.128	-2.16±0.126	0.324	8.262	3.418
24	HD 283447	Binary ^f	YSO	7.692±0.085	10.253±0.843	-25.119±0.301	46	7.805±0.141	8.932±0.39	-29.054±0.25	0.514	9.984	1.795
24				7.70±0.19	8.3±0.50	-23.6±0.5	49						
25	V1271 Tau		YSO	7.418±0.025	22±2	-45.7±2.1	35	7.307±0.052	19.88±0.111	-45.515±0.063	0.0	11.438	1.122
26	V811 Tau		YSO	7.223±0.057	20±2	-47.9±6.9	35	7.215±0.04	19.879±0.077	-44.511±0.05	0.0	12.087	1.552
27	V1065 Tau		YSO	7.382±0.031	17.3±0.7	-44.8±1.8	35	7.221±0.048	16.38±0.084	-47.044±0.054	0.0	11.968	1.437
28	V1282 Tau	Binary ^f	YSO	7.324±0.044	17.1±1	-45.4±0.7	35	7.209±0.051	20.641±0.1	-45.881±0.059	0.0	10.421	1.041
29	[SVS76] Ser 14		YSO	2.313±0.078	3.634±0.05	-8.864±0.127	42	2.241±0.076	2.98±0.13	-8.002±0.113	0.431	14.977	2.896
30	2MASS J18300065+0113402	Binary ^g	YSO	2.638±0.118	1.573±0.07	-6.513±0.152	42	1.858±0.844	4.97±1.872	-3.939±2.08	3.556	19.942	4.003
31	NAME W 40 IRS 5		YSO	2.302±0.063	0.186±0.053	-6.726±0.121	42	2.053±0.212	0.546±0.401	-7.213±0.339	0.787	12.128	3.294
32	GBS-VLA J183123.62-020535.8		YSO	2.186±0.076	-0.258±0.058	-7.514±0.135	42				4.644	17.808	5.146
33	2MASS J18312601-0205169		YSO	2.372±0.12	4.586±0.074	-7.946±0.167	42	3.212±0.461	1.484±0.889	-5.098±0.733	3.0	16.452	4.914
34	2MASS J18312745-0205118		YSO	2.385±0.098	-0.33±0.049	-7.746±0.111	42	2.006±0.225	-1.507±0.469	-8.627±0.508	1.275	17.236	4.971
35	2MASS J16255609-2430148		YSO	7.33±0.112	-9.78±0.09	-25.11±0.2	40	7.561±0.143	-7.055±0.35	-25.498±0.225	0.661	16.135	4.478
36	2MASS J16255752-2430317		YSO	7.404±0.143	-7.26±0.04	-25.29±0.07	40	7.261±0.085	-7.343±0.209	-25.022±0.13	0.41	14.392	3.365
37	2MASS J16263416-2423282	Binary ^f	YSO	7.249±0.091	-2.05±0.02	-26.72±0.04	40	8.166±0.112	-2.17±0.253	-23.557±0.162	0.65	14.137	4.208
38	CoKu HP Tau G2		YSO	6.145±0.029	11.248±0.022	-15.686±0.013	46	6.026±0.048	11.873±0.138	-9.985±0.08	0.0	10.51	1.874
38				6.2±0.03	13.85±0.03	-15.4±0.2	14						
39	Haro 1-6		YSO	7.385±0.234	-19.63±0.19	-26.92±0.13	40	7.446±0.067	-20.184±0.191	-26.765±0.119	0.178	12.238	3.227
40	2MASS J16264375-2416333		YSO	7.16±0.152	-10.48±0.16	-38.99±0.35	40	6.637±0.499	-9.741±1.106	-24.773±0.693	1.886	19.399	3.983
41	2MASS J16264923-2420029		YSO	7.232±0.068	-11.62±0.06	-18.3±0.15	40				9.28	19.031	3.839
42	2MASS J16273084-2447268		YSO	7.327±0.125	-4.41±0.11	-28.79±0.33	40	6.515±0.286	-5.209±0.63	-27.414±0.408	1.513	17.764	4.507

Table 1 continued on next page

Table 1 (continued)

Num	Main name in SIMBAD	Binary	Type	VLBI ϖ (mas)	VLBI μ_x (mas yr ⁻¹)	VLBI μ_y (mas yr ⁻¹)	Ref. ^a	<i>Gaia</i> ϖ (mas)	<i>Gaia</i> μ_x ^b (mas yr ⁻¹)	<i>Gaia</i> μ_y ^b (mas yr ⁻¹)	Noise_sig ^c	Gmag ^d (mag)	bp-rp ^e (mag)
43	2MASS J16303563-2434188	Binary ^g	YSO	7.206±0.08	-7.69±0.02	-26.04±0.04	40	7.551±0.083	-6.547±0.141	-28.693±0.104	0.12	11.774	2.193
44	2MASS J16315211-2456156		YSO	6.676±0.046	-6.38±0.03	-22.74±0.04	40	6.007±0.338	-7.568±0.567	-22.208±0.426	1.072	18.274	3.773
45	DoAr 51	Binary ^g	YSO	6.983±0.05	-4.8±0.08	-23.11±0.11	40	7.248±0.384	-5.196±1.068	-21.538±0.718	1.367	12.524	2.629
46	V1096 Tau	Binary ^g	YSO	8.055±0.535	2.089±0.73	-16.167±0.711	46	7.337±0.068	7.44±0.156	-23.835±0.105	0.167	12.223	2.741
46				7.924±1.334	7.14±2.149	-28.765±2.186	46						
47	V1098 Tau		YSO	8.07±0.31	11.148±0.175	-27.327±0.172	46				16.17	11.132	2.33
48	V410 Tau	Binary ^g	YSO	7.751±0.027	8.703±0.017	-24.985±0.02	46	7.667±0.053	8.683±0.128	-25.1±0.061	0.0	10.321	1.557
49	V1023 Tau	Binary ^g	YSO	7.686±0.032	8.371±0.02	-25.49±0.02	46	7.951±0.152	8.296±0.356	-25.309±0.229	0.58	11.652	2.367
49				7.53±0.03	3.785±0.044	-28.9±0.3	9						
50	V1201 Tau	Binary ^g	YSO	6.363±0.069	10.839±0.05	-13.235±0.058	46	6.166±0.046	10.469±0.104	-14.544±0.077	0.0	10.725	1.81
51	HD 283641		YSO	6.285±0.07	10.913±0.037	-16.772±0.044	46	6.212±0.084	10.612±0.173	-17.047±0.134	0.2	10.799	1.719
52	XZ Tau	Binary ^g	YSO	6.793±0.025	10.858±0.027	-16.264±0.06	46				5.03	12.908	2.773
53	V807 Tau	Binary ^g	YSO	7.899±0.105	8.573±0.068	-28.774±0.201	46	8.834±0.659	9.559±1.235	-20.23±0.989	2.994	10.749	1.965
54	V1110 Tau	Binary ^f	YSO	11.881±0.149	-52.705±0.062	-11.321±0.066	46	11.6±0.04	-52.267±0.093	-11.342±0.07	0.0	9.959	1.189
55	V999 Tau		YSO	6.972±0.197	9.533±0.218	-15.684±0.198	46	8.138±0.391	5.493±0.641	-18.99±0.385	1.967	13.515	2.97
56	V1000 Tau	Binary ^g	YSO	7.324±0.132	6.01±0.235	-17.72±0.159	46				15.396	13.532	3.359
57	HD 282630		YSO	7.061±0.125	3.897±0.113	-24.21±0.132	46	6.263±0.079	4.307±0.154	-24.132±0.076	0.0	10.333	1.259
58	HD 283572		YSO	7.722±0.057	8.853±0.096	-26.491±0.113	46	7.673±0.052	9.011±0.115	-26.385±0.072	0.0	8.796	1.07
58				7.78±0.04	7.819±0.053	-26.6±0.1	9						
59	V1229 Ori	Binary ^g	YSO	2.567±0.051	2.38±0.08	0.55±0.14	41	2.519±0.054	2.13±0.1	0.781±0.085	0.0	12.259	1.377
60	MT Ori		YSO	2.646±0.041	3.82±0.1	1.6±0.17	41	2.404±0.053	3.772±0.096	2.345±0.08	0.0	11.324	1.61
61	* tet01 Ori E	Binary ^f	YSO	2.557±0.051	1.45±0.03	1.02±0.08	41	2.388±0.095	1.614±0.122	1.228±0.114	0.0	9.645	1.455
62	* tet01 Ori A	Binary ^f	YSO	2.626±0.1	4.81±0.1	-2.53±0.12	41	2.373±0.105	1.536±0.158	0.123±0.139	0.227	6.609	0.151
63	Brun 656	Binary ^g	YSO	2.708±0.21	2.36±0.69	0.06±1.05	41	2.114±0.046	0.111±0.073	-3.978±0.08	0.0	10.483	1.489
64	V1699 Ori		YSO	2.493±0.049	1.76±0.05	-0.89±0.16	41	2.555±0.262	1.551±0.425	-1.034±0.366	1.19	18.396	2.388
65	V1961 Ori		YSO	2.533±0.027	-7.22±0.06	-0.99±0.08	41	2.546±0.041	-7.194±0.089	-1.037±0.09	0.0	11.609	1.61
66	V1321 Ori		YSO	2.509±0.044	0.06±0.12	6.95±0.16	41	2.431±0.037	0.259±0.059	7.103±0.057	0.0	10.13	1.623
67	Brun 334	Binary ^f	YSO	2.591±0.046	-4.01±0.08	-1.17±0.07	41	2.495±0.043	-3.848±0.1	-0.958±0.083	0.0	10.818	1.58
68	HD 37150		YSO	2.536±0.046	1.32±0.05	-0.56±0.12	41	2.706±0.061	1.712±0.133	-0.194±0.106	0.233	6.508	-0.284
69	V1046 Ori	Binary ^f	YSO	2.643±0.075	1.88±0.09	1.2±0.14	41	0.447±0.171	0.459±0.394	2.511±0.384	0.62	6.532	-0.199
70	V363 Ori		YSO	2.575±0.389	0.33±0.05	-1.34±0.43	41	3.181±0.182	2.606±0.343	-0.431±0.31	1.361	13.574	2.552
71	V1727 Ori		YSO	2.312±0.207	2.54±0.3	-1.3±0.64	41	2.196±0.233	2.872±0.399	-1.016±0.347	1.622	13.783	2.212
72	V621 Ori		YSO	2.422±0.034	0.19±0.44	-0.97±0.27	41	2.691±0.11	0.665±0.144	-1.305±0.114	0.368	14.183	2.694
73	HD 294300	Binary ^g	YSO	3.303±0.353	-4.92±0.66	4.67±1.37	41	2.789±0.12	2.775±0.172	-3.188±0.132	0.195	9.718	1.014
74	HD 290862	Binary ^g	YSO	2.197±0.545	0.35±0.27	0.83±0.83	41	2.177±0.064	-0.257±0.109	-0.652±0.104	0.16	10.18	1.072
75	2MASS J05420800-0812028		YSO	2.315±0.072	0.13±0.25	-1.05±0.18	41	1.589±0.925	0.466±1.955	-4.241±2.303	3.01	20.354	4.26
76	GBS-VLA J054643.62+000528.3		YSO	2.608±0.047	-1.02±0.02	-0.52±0.15	41	2.381±0.062	-0.54±0.114	-1.183±0.103	0.33	13.992	2.79
77	TYC 5346-538-1		YSO	2.348±0.069	0.68±0.09	-0.51±0.25	41	2.393±0.06	0.827±0.145	-0.322±0.146	0	10.647	1.21
78	[SSC75] M 78 11		YSO	2.547±0.034	0.01±0.01	-0.49±0.08	41	2.494±0.041	0.29±0.076	-1.185±0.072	0	12.513	1.84
79	[BCB89] IRS 11	Binary ^g	YSO	1.865±0.105	-0.43±0.16	1.03±0.42	41	2.613±0.307	0.649±0.407	-1.415±0.407	0.96	18.093	3.40
80	[BCB89] IRS 15	Binary ^g	YSO	2.223±0.121	0.04±0.31	0.2±0.43	41	2.637±0.152	0.029±0.221	-0.646±0.209	0.73	16.110	4.02
81	2MASS J05413786-0154323	Binary ^g	YSO	2.804±0.032	0.55±0.1	-0.1±0.15	41	2.780±0.238	-1.11±0.449	-0.754±0.386	0.96	17.259	2.77
82	EM* LkHA 101	Binary ^g	YSO	1.87±0.1	1.86±0.04	-5.7±0.05	13	1.614±0.078	2.015±0.154	-5.320±0.115	0.38	14.854	2.977
83	V913 Per		YSO	3.119±0.104	2.458±0.047	-7.272±0.133	48	3.708±0.262	5.039±0.482	-7.111±0.281	1.095	14.696	2.914
84	V918 Per	Binary ^g	YSO	3.129±0.512	4.857±0.335	-6.75±0.488	48	1.852±0.333	-3.321±0.602	-9.831±0.439	0.818	12.097	2.209
85	CI* IC 348 LRL 11	Binary ^g	YSO	2.68±0.076	2.37±0.08	-8.271±0.16	48	2.665±0.117	1.814±0.214	-9.807±0.123	0.475	14.087	3.019
86	IRAS 20126+4104		YSO	0.61±0.02			18	0.886±0.368	-3.913±0.611	-4.578±0.701	1.548	19.19	2.355
86				0.75±0.092	-4.15±0.51	-4.07±0.51	36						
87	HD 36705	Binary ^g	YSO	66.75±0.45	48.927±2.805	137.5±7.5	2	65.32±0.144	29.15±0.251	164.421±0.299	0.85	6.674	1.1

Table 1 continued on next page

Table 1 (*continued*)

Num	Main name in SIMBAD	Binary	Type	VLBI ϖ	VLBI μ_x	VLBI μ_y	Ref. ^a	<i>Gaia</i> ϖ	<i>Gaia</i> μ_x ^b	<i>Gaia</i> μ_y ^b	Noise_sig ^c	Gmag ^d	bp-rp ^e
				(mas)	(mas yr ⁻¹)	(mas yr ⁻¹)		(mas)	(mas yr ⁻¹)	(mas yr ⁻¹)		(mag)	(mag)
88	T Tau	Binary ^g	YSO	6.723±0.046	6.79±0.432	-11.131±0.444	46	6.929±0.058	11.356±0.122	-14.837±0.1	0.12	9.627	1.653
88				6.90±0.09	12.35±0.04	-12.80±0.06	50						
89	V404 Cyg	Binary ^f	Other Star	0.418±0.024	-5.04±0.02	-7.64±0.03	16	0.439±0.1	-5.769±0.175	-7.845±0.173	0.501	17.188	2.874
90	LS I +61 303	Binary ^f	Other Star	0.26±0.61	0.967±0.26	-1.21±0.32	3	0.38±0.038	-0.296±0.041	-0.079±0.067	0.0	10.393	1.29
91	* bet Per	Binary ^f	Other Star	33.32±0.73	2.787±0.136	-0.64±0.18	3				3.025	4.34	2.378
91				34.7±0.6	2.7±0.07	-0.8±0.09	19						
92	UX Ari	Binary ^f	Other Star	19.37±0.39	41.229±0.184	-104.01±0.2	3	19.813±0.228	46.317±0.493	-101.899±0.359	0.895	6.329	1.193
92				19.9±	44.96±0.13	-102.33±0.09	19						
93	HD 22468	Binary ^f	Other Star	33.88±0.47	-31.588±0.33	-161.69±0.31	3	33.753±0.087	-32.894±0.131	-161.772±0.118	0.195	5.6	1.216
94	BH CVn	Binary ^f	Other Star	22.21±0.45	85.496±0.131	-9.22±0.16	3	21.669±0.16	85.607±0.189	-9.711±0.148	0.702	4.73	0.633
95	* sig CrB	Binary ^f	Other Star	43.93±0.1	-267.05±0.037	-86.66±0.05	3	44.135±0.064	-268.325±0.096	-86.925±0.146	0.356	5.407	0.794
96	HD 226868	Binary ^f	Other Star	0.73±0.3	-3.787±0.172	-6.25±0.21	3	0.422±0.032	-3.882±0.048	-6.171±0.054	0.0	8.523	1.271
96				0.539±0.033	-3.78±0.06	-6.4±0.12	20						
97	HD 199178		Other Star	8.59±0.33	26.595±0.407	-1.24±0.43	3	8.902±0.04	26.323±0.061	-0.742±0.066	0.0	7.005	1.018
98	AR Lac	Binary ^f	Other Star	23.97±0.37	-52.08±0.126	47.03±0.19	3	23.433±0.03	-52.19±0.043	47.19±0.046	0.0	5.894	0.958
99	IM Peg	Binary ^f	Other Star	10.28±0.62	-20.587±0.459	-27.53±0.4	3	10.05±0.091	-20.719±0.137	-26.851±0.131	0.277	5.655	1.355
99				10.37±0.07	-20.83±0.09	-27.27±0.09	25						
100	AM Her	Binary ^f	Other Star	11.29±0.08	-46.02±0.22	28.83±0.18	47	11.395±0.018	-45.957±0.034	28.046±0.034	0.0	13.58	1.01
101	TVLM 513-46	Binary ^g	Other Star	93.27±0.18	-39.75±0.074	-65.5±0.07	44	93.45±0.195	-43.766±0.349	-63.997±0.329	1.105	16.53	5.031
101				92.92±0.23	-39.225±0.111	-65.47±0.12	29						
102	SS Cyg	Binary ^f	Other Star	8.8±0.12	112.42±0.07	33.38±0.07	31	8.724±0.049	112.373±0.113	33.589±0.094	0.0	11.689	1.163
103	PSR J0437-4715	Binary ^f	Pulsar	6.396±0.054	121.679±0.052	-71.82±0.086	10	8.325±0.678	122.864±1.197	-71.166±1.67	0.0	20.41	1.548
104	PSR J1023+0038	Binary ^f	Pulsar	0.731±0.022	4.76±0.03	-17.34±0.04	24	0.728±0.143	4.751±0.135	-17.348±0.135	0.0	16.265	0.776
105	PN K 3-35		AGB	0.26±0.04	-3.11±0.10	-5.93±0.07	1	0.384±0.125	-2.935±0.149	-3.351±0.185	2.410	17.546	2.159
106	IRAS 20143+3634		YSO	0.367±0.037	-2.99±0.16	-4.37±0.43	4	0.320±0.071	-3.113±0.108	-2.923±0.147	0.000	16.932	1.785
107	BD+40 4220	Binary ^f	Other Star	0.61±0.22	-1.64±0.98	-7.16±0.98	6	0.638±0.056	-3.083±0.101	-4.085±0.080	0.000	8.240	2.336
108	SV Peg		AGB	3.00±0.06	11.59±0.54	-8.63±0.44	15	1.124±0.283	15.244±0.487	-5.989±0.498	628.467	7.846	

^a References: 1–Tafaya et al. (2011), 2–Guirado et al. (1997), 3–Lestrade et al. (1999), 4–Burns et al. (2014), 5–Vlemmings et al. (2003), 6–Dzib et al. (2013), 7–Kurayama et al. (2005), 8–Vlemmings & van Langevelde (2007), 9–Torres et al. (2007), 10–Deller et al. (2008), 11–Choi et al. (2008), 12–Nakagawa et al. (2008), 13–Dzib et al. (2018), 14–Torres et al. (2009), 15–Sudou et al. (2019), 16–Miller-Jones et al. (2009), 17–Asaki et al. (2010), 18–Moscadelli et al. (2011), 19–Peterson et al. (2011), 20–Reid et al. (2011), 21–Nyu et al. (2011), 22–Zhang et al. (2012c), 23–Zhang et al. (2012a), 24–Deller et al. (2012), 25–Ratner et al. (2012), 26–Kamezaki et al. (2012), 27–Imai et al. (2012), 28–Kusuno et al. (2013), 29–Forbrich et al. (2013), 30–Imai et al. (2013), 31–Miller-Jones et al. (2013), 32–Min et al. (2014), 33–Nakagawa et al. (2014), 34–Kamezaki et al. (2014), 35–Melis et al. (2014), 36–Nagayama et al. (2015), 37–Kamezaki et al. (2016b), 38–Kamezaki et al. (2016a), 39–Nakagawa et al. (2016), 40–Ortiz-León et al. (2017a), 41–Kounkel et al. (2017), 42–Ortiz-León et al. (2017b), 43–Zhang et al. (2017), 44–Gawroński et al. (2017), 45–Xu et al. (2018), 46–Galli et al. (2018), 47–Gawroński et al. (2018), 48–Ortiz-León et al. (2018), 49–Torres et al. (2012), 50–Loinard et al. (2007)

^b $\mu_x = \mu_\alpha \cos \delta$, $\mu_y = \mu_\delta$

^c astrometric “excess noise”

^d G-band mean magnitude

^e *Gaia* color: $G_{BP}-G_{RP}$

^f The binary was identified by SIMBAD database.

^g The binary was identified by each reference paper.

REFERENCES

- Asaki, Y., Deguchi, S., Imai, H., et al. 2010, *ApJ*, 721, 267, doi: [10.1088/0004-637X/721/1/267](https://doi.org/10.1088/0004-637X/721/1/267)
- Bobylev, V. V. 2018, arXiv e-prints, arXiv:1812.07838. <https://arxiv.org/abs/1812.07838>
- Burns, R. A., Yamaguchi, Y., Handa, T., et al. 2014, *PASJ*, 66, 102, doi: [10.1093/pasj/psu094](https://doi.org/10.1093/pasj/psu094)
- Choi, Y. K., Hirota, T., Honma, M., et al. 2008, *PASJ*, 60, 1007. <https://arxiv.org/abs/0808.0641>
- Deller, A. T., Verbiest, J. P. W., Tingay, S. J., & Bailes, M. 2008, *ApJL*, 685, L67, doi: [10.1086/592401](https://doi.org/10.1086/592401)
- Deller, A. T., Archibald, A. M., Brisken, W. F., et al. 2012, *ApJL*, 756, L25, doi: [10.1088/2041-8205/756/2/L25](https://doi.org/10.1088/2041-8205/756/2/L25)
- Deming, W. E. 1943, *Revue De L Institut International De Statistique*, 34, 112
- Dzib, S. A., Ortiz-León, G. N., Loinard, L., et al. 2018, *ApJ*, 853, 99, doi: [10.3847/1538-4357/aaa431](https://doi.org/10.3847/1538-4357/aaa431)
- Dzib, S. A., Rodríguez, L. F., Loinard, L., et al. 2013, *ApJ*, 763, 139, doi: [10.1088/0004-637X/763/2/139](https://doi.org/10.1088/0004-637X/763/2/139)
- Feigelson, E. D., & Babu, G. J. 2012, *Modern Statistical Methods for Astronomy*
- Forbrich, J., Berger, E., & Reid, M. J. 2013, *ApJ*, 777, 70, doi: [10.1088/0004-637X/777/1/70](https://doi.org/10.1088/0004-637X/777/1/70)
- Gaia Collaboration, Brown, A. G. A., Vallenari, A., et al. 2018, *A&A*, 616, A1, doi: [10.1051/0004-6361/201833051](https://doi.org/10.1051/0004-6361/201833051)
- Galli, P. A. B., Loinard, L., Ortiz-León, G. N., et al. 2018, *ApJ*, 859, 33, doi: [10.3847/1538-4357/aabf91](https://doi.org/10.3847/1538-4357/aabf91)
- Gawroński, M. P., Goździewski, K., & Katarzyński, K. 2017, *MNRAS*, 466, 4211, doi: [10.1093/mnras/stw3329](https://doi.org/10.1093/mnras/stw3329)
- Gawroński, M. P., Goździewski, K., Katarzyński, K., & Rycyk, G. 2018, *MNRAS*, 475, 1399, doi: [10.1093/mnras/stx3175](https://doi.org/10.1093/mnras/stx3175)
- Guirado, J. C., Reynolds, J. E., Lestrade, J.-F., et al. 1997, *ApJ*, 490, 835
- Imai, H., Kurayama, T., Honma, M., & Miyaji, T. 2013, *PASJ*, 65, 28, doi: [10.1093/pasj/65.2.28](https://doi.org/10.1093/pasj/65.2.28)
- Imai, H., Sakai, N., Nakanishi, H., et al. 2012, *PASJ*, 64, 142, doi: [10.1093/pasj/64.6.142](https://doi.org/10.1093/pasj/64.6.142)
- Jennings, R. J., Kaplan, D. L., Chatterjee, S., Cordes, J. M., & Deller, A. T. 2018, *ApJ*, 864, 26, doi: [10.3847/1538-4357/aad084](https://doi.org/10.3847/1538-4357/aad084)
- Kamezaki, T., Kurayama, T., Nakagawa, A., et al. 2014, *PASJ*, 66, 107, doi: [10.1093/pasj/psu112](https://doi.org/10.1093/pasj/psu112)
- Kamezaki, T., Nakagawa, A., Omodaka, T., et al. 2016a, *PASJ*, 68, 75, doi: [10.1093/pasj/psw068](https://doi.org/10.1093/pasj/psw068)
- . 2012, *PASJ*, 64, 7. <https://arxiv.org/abs/1201.3721>
- . 2016b, *PASJ*, 68, 71, doi: [10.1093/pasj/psv030](https://doi.org/10.1093/pasj/psv030)
- Kounkel, M., Hartmann, L., Loinard, L., et al. 2017, *ApJ*, 834, 142, doi: [10.3847/1538-4357/834/2/142](https://doi.org/10.3847/1538-4357/834/2/142)
- Kounkel, M., Covey, K., Suárez, G., et al. 2018, *AJ*, 156, 84, doi: [10.3847/1538-3881/aad1f1](https://doi.org/10.3847/1538-3881/aad1f1)
- Kurayama, T., Sasao, T., & Kobayashi, H. 2005, *ApJL*, 627, L49, doi: [10.1086/432051](https://doi.org/10.1086/432051)
- Kusuno, K., Asaki, Y., Imai, H., & Oyama, T. 2013, *ApJ*, 774, 107, doi: [10.1088/0004-637X/774/2/107](https://doi.org/10.1088/0004-637X/774/2/107)
- Le Bouquin, J.-B., Lacour, S., Renard, S., et al. 2009, *A&A*, 496, L1, doi: [10.1051/0004-6361/200811579](https://doi.org/10.1051/0004-6361/200811579)
- Lestrade, J.-F., Preston, R. A., Jones, D. L., et al. 1999, *A&A*, 344, 1014
- Levesque, E. M., Massey, P., Olsen, K. A. G., et al. 2005, *ApJ*, 628, 973, doi: [10.1086/430901](https://doi.org/10.1086/430901)
- Lindgren, L., Hernández, J., Bombrun, A., et al. 2018, *A&A*, 616, A2, doi: [10.1051/0004-6361/201832727](https://doi.org/10.1051/0004-6361/201832727)
- Loinard, L., Torres, R. M., Mioduszewski, A. J., et al. 2007, *ApJ*, 671, 546, doi: [10.1086/522493](https://doi.org/10.1086/522493)
- Luri, X., Brown, A. G. A., Sarro, L. M., et al. 2018, *A&A*, 616, A9, doi: [10.1051/0004-6361/201832964](https://doi.org/10.1051/0004-6361/201832964)
- Melis, C., Reid, M. J., Mioduszewski, A. J., Stauffer, J. R., & Bower, G. C. 2014, *Science*, 345, 1029. <https://arxiv.org/abs/1408.6544>
- Millan-Gabet, R., Pedretti, E., Monnier, J. D., et al. 2005, *ApJ*, 620, 961, doi: [10.1086/427163](https://doi.org/10.1086/427163)
- Miller-Jones, J. C. A., Jonker, P. G., Dhawan, V., et al. 2009, *ApJL*, 706, L230, doi: [10.1088/0004-637X/706/2/L230](https://doi.org/10.1088/0004-637X/706/2/L230)
- Miller-Jones, J. C. A., Sivakoff, G. R., Knigge, C., et al. 2013, *Science*, 340, 950, doi: [10.1126/science.1237145](https://doi.org/10.1126/science.1237145)
- Min, C., Matsumoto, N., Kim, M. K., et al. 2014, *PASJ*, 66, 38, doi: [10.1093/pasj/psu003](https://doi.org/10.1093/pasj/psu003)
- Monnier, J. D., Danchi, W. C., Hale, D. S., Tuthill, P. G., & Townes, C. H. 2000, *ApJ*, 543, 868, doi: [10.1086/317127](https://doi.org/10.1086/317127)
- Moscadelli, L., Cesaroni, R., Rioja, M. J., Dodson, R., & Reid, M. J. 2011, *A&A*, 526, A66, doi: [10.1051/0004-6361/201015641](https://doi.org/10.1051/0004-6361/201015641)
- Mowlavi, N., Lecoœur-Taïbi, I., Lebzelter, T., et al. 2018, *A&A*, 618, A58, doi: [10.1051/0004-6361/201833366](https://doi.org/10.1051/0004-6361/201833366)
- Nagayama, T., Omodaka, T., Handa, T., et al. 2015, *PASJ*, 67, 66, doi: [10.1093/pasj/psu133](https://doi.org/10.1093/pasj/psu133)
- Nakagawa, A., Kurayama, T., Matsui, M., et al. 2016, *PASJ*, 68, 78, doi: [10.1093/pasj/psw069](https://doi.org/10.1093/pasj/psw069)
- Nakagawa, A., Tsushima, M., Ando, K., et al. 2008, *PASJ*, 60, 1013, doi: [10.1093/pasj/60.5.1013](https://doi.org/10.1093/pasj/60.5.1013)
- Nakagawa, A., Omodaka, T., Handa, T., et al. 2014, *PASJ*, 66, 101, doi: [10.1093/pasj/psu103](https://doi.org/10.1093/pasj/psu103)
- Nyu, D., Nakagawa, A., Matsui, M., et al. 2011, *PASJ*, 63, 63, doi: [10.1093/pasj/63.1.63](https://doi.org/10.1093/pasj/63.1.63)
- Ortiz-León, G. N., Loinard, L., Kounkel, M. A., et al. 2017a, *ApJ*, 834, 141, doi: [10.3847/1538-4357/834/2/141](https://doi.org/10.3847/1538-4357/834/2/141)

- Ortiz-León, G. N., Dzib, S. A., Kounkel, M. A., et al. 2017b, *ApJ*, 834, 143, doi: [10.3847/1538-4357/834/2/143](https://doi.org/10.3847/1538-4357/834/2/143)
- Ortiz-León, G. N., Loinard, L., Dzib, S. A., et al. 2018, ArXiv e-prints. <https://arxiv.org/abs/1808.03499>
- Peterson, W. M., Mutel, R. L., Lestrade, J.-F., Güdel, M., & Goss, W. M. 2011, *ApJ*, 737, 104, doi: [10.1088/0004-637X/737/2/104](https://doi.org/10.1088/0004-637X/737/2/104)
- R Core Team. 2013, *R: A Language and Environment for Statistical Computing*, R Foundation for Statistical Computing, Vienna, Austria
- Ratner, M. I., Bartel, N., Bietenholz, M. F., et al. 2012, *ApJS*, 201, 5, doi: [10.1088/0067-0049/201/1/5](https://doi.org/10.1088/0067-0049/201/1/5)
- Reid, M. J., & Honma, M. 2014, *ARA&A*, 52, 339, doi: [10.1146/annurev-astro-081913-040006](https://doi.org/10.1146/annurev-astro-081913-040006)
- Reid, M. J., McClintock, J. E., Narayan, R., et al. 2011, *ApJ*, 742, 83, doi: [10.1088/0004-637X/742/2/83](https://doi.org/10.1088/0004-637X/742/2/83)
- Richards, A. M. S., Etoka, S., Gray, M. D., et al. 2012, *A&A*, 546, A16, doi: [10.1051/0004-6361/201219514](https://doi.org/10.1051/0004-6361/201219514)
- Riess, A. G., Casertano, S., Yuan, W., et al. 2018, *ApJ*, 861, 126, doi: [10.3847/1538-4357/aac82e](https://doi.org/10.3847/1538-4357/aac82e)
- Sanna, A., Reid, M. J., Dame, T. M., Menten, K. M., & Brunthaler, A. 2017, *Science*, 358, 227, doi: [10.1126/science.aan5452](https://doi.org/10.1126/science.aan5452)
- Stassun, K. G., & Torres, G. 2018, *ApJ*, 862, 61, doi: [10.3847/1538-4357/aaca6c](https://doi.org/10.3847/1538-4357/aaca6c)
- Sudou, H., Omodaka, T., Murakami, K., et al. 2019, *PASJ*, 71, 16, doi: [10.1093/pasj/psy133](https://doi.org/10.1093/pasj/psy133)
- Tafoya, D., Imai, H., Gomez, Y., et al. 2011, *PASJ*, 63, 71, doi: [10.1093/pasj/63.1.71](https://doi.org/10.1093/pasj/63.1.71)
- Taylor, M. B. 2005, in *Astronomical Society of the Pacific Conference Series*, Vol. 347, *Astronomical Data Analysis Software and Systems XIV*, ed. P. Shopbell, M. Britton, & R. Ebert, 29
- Torres, R. M., Loinard, L., Mioduszewski, A. J., et al. 2012, *ApJ*, 747, 18, doi: [10.1088/0004-637X/747/1/18](https://doi.org/10.1088/0004-637X/747/1/18)
- Torres, R. M., Loinard, L., Mioduszewski, A. J., & Rodríguez, L. F. 2007, *ApJ*, 671, 1813, doi: [10.1086/522924](https://doi.org/10.1086/522924)
- . 2009, *ApJ*, 698, 242, doi: [10.1088/0004-637X/698/1/242](https://doi.org/10.1088/0004-637X/698/1/242)
- Tukey, J. W. 1977, *Exploratory data analysis*
- Vlemmings, W. H. T., & van Langevelde, H. J. 2007, *A&A*, 472, 547, doi: [10.1051/0004-6361:20077897](https://doi.org/10.1051/0004-6361:20077897)
- Vlemmings, W. H. T., van Langevelde, H. J., Diamond, P. J., Habing, H. J., & Schilizzi, R. T. 2003, *A&A*, 407, 213, doi: [10.1051/0004-6361:20030766](https://doi.org/10.1051/0004-6361:20030766)
- Wenger, M., Ochsenbein, F., Egret, D., et al. 2000, *A&AS*, 143, 9, doi: [10.1051/aas:2000332](https://doi.org/10.1051/aas:2000332)
- Xu, S., Zhang, B., Reid, M. J., et al. 2018, *ApJ*, 859, 14, doi: [10.3847/1538-4357/aabba6](https://doi.org/10.3847/1538-4357/aabba6)
- York, D., Evensen, N. M., Martínez, M. L., & De Basabe Delgado, J. 2004, *American Journal of Physics*, 72, 367, doi: [10.1119/1.1632486](https://doi.org/10.1119/1.1632486)
- Zhang, B., Reid, M. J., Menten, K. M., & Zheng, X. W. 2012a, *ApJ*, 744, 23, doi: [10.1088/0004-637X/744/1/23](https://doi.org/10.1088/0004-637X/744/1/23)
- Zhang, B., Reid, M. J., Menten, K. M., Zheng, X. W., & Brunthaler, A. 2012b, *A&A*, 544, A42, doi: [10.1051/0004-6361/201219587](https://doi.org/10.1051/0004-6361/201219587)
- . 2012c, *A&A*, 544, A42, doi: [10.1051/0004-6361/201219587](https://doi.org/10.1051/0004-6361/201219587)
- Zhang, B., Zheng, X., Reid, M. J., et al. 2017, *ApJ*, 849, 99, doi: [10.3847/1538-4357/aa8ee9](https://doi.org/10.3847/1538-4357/aa8ee9)
- Zinn, J. C., Pinsonneault, M. H., Huber, D., & Stello, D. 2018, ArXiv e-prints. <https://arxiv.org/abs/1805.02650>